Experiments on three-dimensional instabilities in a confined flow generated by a rotating lid

Jens Nørkær Sørensen[1], Igor Naumov[2] and Robert Mikkelsen[1]

[1] Department of Mechanical Engineering, Technical University of Denmark

[2] Institute of Thermophysics, SB RAS1, Novosibirsk, 630090, Russia

E-mail: jns@mek.dtu.dk

Abstract. Three-dimensional instabilities occurring in a swirling flow between a rotating lid and a stationary cylinder is studied experimentally. Two model parameters govern the flow: The ratio of container height to disk radius, h, and the Reynolds number, Re, based on the disk angular velocity, cylinder radius and kinematic viscosity of the liquid. Azimuthal instabilitites and onset of three-dimensional flow behaviour is measured by combining the high spatial resolution of Particle Image Velocimetry (PIV) and the temporal accuracy of Laser Doppler Anemometry (LDA). The transition scenario from steady and axisymmetric flow to unsteady and three-dimensional flow is investigated for $1 \le h \le 3.5$. The flow is characterized by the development of azimuthal modes of different wave numbers. A range of different modes is detected and critical Reynolds numbers and associated frequencies are identified and compared to the numerical stability analysis of Gelfgat et al. [J. of Fluid Mechanics 438, (2001)].

1. Introduction

In the present work we study the onset of three-dimensional instabilities occurring in a rotating flow in a closed cylinder, driven by rotating one of the end walls. In spite of its simplicity, the lid-driven rotating flow exhibits a rich dynamic behaviour, including vortex break down and a complicated route to chaos. The rotating lid forces the fluid to perform a rotating motion around the center axis. Due to centrifugal forces it moves the fluid close to the lid away from the center, causing as a result a meridional circulation. The fluid then travels downwards along the outer wall and turns inwards near the fixed bottom. Close to the center axis it rises vertically, forms a concentrated vortex structure due to the conservation of angular momentum, and returns to the rotating lid. Changes of the flow structures depend on two parameters (see Figs. 1 and 2): The aspect ratio h (ratio of the container height to the disk radius H/R) and the Reynolds number $Re = \Omega R^2/\nu$, where Ω is the angular velocity of the disk and ν is the kinematic viscosity of the working fluid.

The swirling lid-driven cavity flow has for more than three decades been the subject of a large number of experimental and computational studies, and is today considered as a classical flow case for studying vortex breakdown and onset of transition. The first experiments by Vogel [1], and later by Ronnenberg [2] and Escudier [3], showed the formation of a concentrated vortex core along the center axis. In the experiment of Escudier [3] the formation and onset of re-circulating bubbles, interpreted as vortex breakdown, were systematically investigated. Based on these pioneering works, a lot of experimental and numerical studies have later been carried out. Among those, Westergaard et al. [4] employed the Particle Image Velocimetry (PIV) technique to study

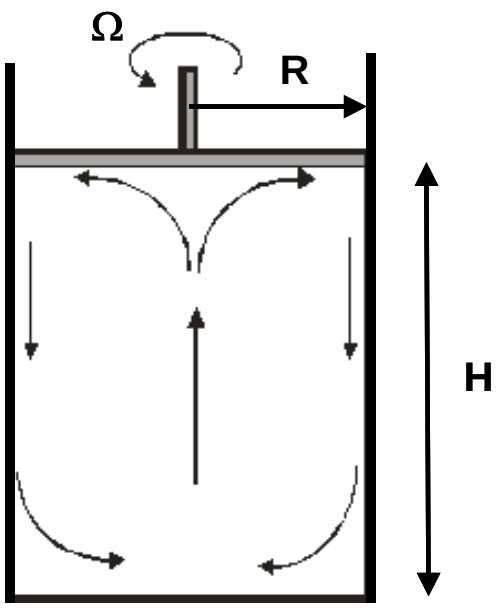

Figure 1. Sketch of the geometry and main flow directions.

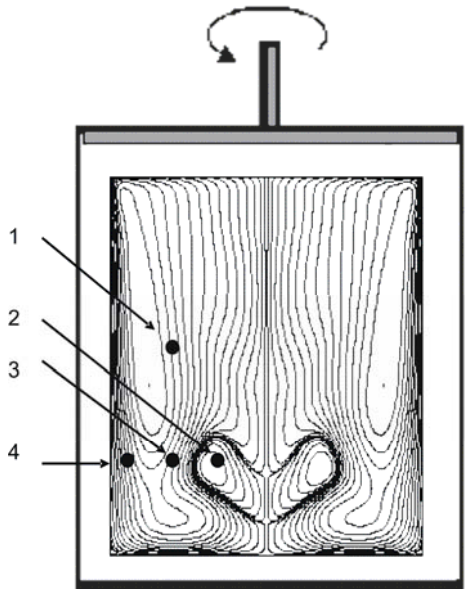

Figure 2. Sketch of flow structures and monitor points for LDA measurements.

onset of re-circulating bubbles. Spohn et al. [5] used the visualization techniques of electrolytic precipitation and fluorescent dye and showed that the vortex-breakdown bubbles appearing in the flow, even at steady and axisymmetric flow conditions, are open and asymmetric at their downstream end. Later experiments are due to Stevens et al. [6] who studied in detail the onset of unsteady axisymmetric flow behaviour. Recently, Sotiropoulos et al. [7] used planar laser-induced fluorescence technique and showed the existence of Lagrangian chaos behaviour within steady vortex-breakdown bubbles.

In a numerical study by Gelfgat et al. [8] a detailed analysis of the onset of non-axisymmetric instabilities as a function of Reynolds number was performed for aspect ratios in the range $1 \le h \le 3.5$. The analysis was carried out using a spectral Galerkin method combined with an eigenvalue analysis to detect the azimuthal wave numbers, *k*, associated with neutral and critical modes. The neutral Reynolds number, $\mathrm{Re}_n(h,k)$, is defined as the lowest Reynolds number at which a particular azimuthal wave, *k*, starts to grow. To the mode *k* is associated a frequency, designated $\omega_n(h,k)$. The critical Reynolds number is defined by $\mathrm{Re}_{cr}(h) = \min_k \mathrm{Re}_n(h,k)$, that is, the most unstable mode can be recognized as that corresponding to the lowest $\mathrm{Re}_n(h,k)$. The neutral and critical Reynolds numbers, and associated frequencies of the perturbations, were computed and several individual modes of instability were identified. The computations were in good agreement with the experimental results of Escudier [3] in the range $1.86 < h < 2.9$. Below $h = 1.86$, however, no experimental results are available for the comparison, and for $2.9 < h < 3.5$ the instabilities did not agree with Escudier's observations. To supplement the visualizations of Escudier [3] and the analysis Gelfgat et al. [8] we have performed a series of experiments to detect critical modes in the rotating cavity using quantitative, non-intrusive experimental techniques.

The purpose of the present work is experimentally to investigate and analyze the appearance of non-axisymmetric instabilities of the swirling flow in a closed cylinder with rotating lid for aspect ratios $1.0 \le h \le 3.5$. This is accomplished by applying a new technique in which measurements using Particle Image Velocimetry (PIV) and Laser Doppler Anemometry (LDA) are simultaneously performed. The use of PIV allows accurate simultaneous measurements of a complete velocity field in a 2-dimensional plane perpendicular to the axis of the cylinder and LDA makes it possible to

determine onset and frequency content of the unsteady flow. Thus, combining the two techniques allows determining the frequency content of the various modes appearing in the unsteady flow domain as a function of the control parameters (*h* and *Re*). We begin by determining the critical Reynolds numbers at which the basic steady and axisymmetric state loses its stability. Next, a detailed analysis is performed in which the different azimuthal modes and frequencies are detected as function of wave number, Reynolds numbers and aspect ratio.

2. Experimental technique and data acquisition

The experiments were carried out in a cylindrical Plexiglas container with an inner diameter of 288 mm (Fig. 1). Both the top and the bottom lid are connected to stepping motors that allow them to be rotated individually. In the present investigation, however, only the top lid is rotated. The top lid is further connected to a stepping motor that may lift it continuously in order to vary the height of the flow domain, *H*. The mechanism can change the aspect ratio between 0 and 6. In the present investigation the aspect ratio is varied in the range from 1 to 3.5. The gap between the rotating disk and the cylinder wall is 0.3 mm. The whole cylindrical container is placed inside a rectangular box of dimensions 700x700x800 mm that is made of glass and filled with tap water, in order to minimize optical aberrations and thermal changes. An 80% glycerin-water mixture was used as working fluid. The viscosity of the fluid was measured at various temperatures in the range from 20^oC to 30^oC. The temperature dependency of the viscosity was approximated by a second order polynomium, with a value of 50 cS at 20^oC and of 31.6 cS at 30^oC. For both the LDA and the PIV measurements polyamide beads with an average diameter of 10 μm were employed as seeding particles.

2.1 *Estimation of accuracy*

The aspect ratio depends on the height from the fixed bottom lid to the rotating upper lid, *H*, and the radius, *R*. With a cylinder radius of 144 mm and an estimated precision of *H* less than 0.2 mm, the error in aspect ratio is less than 0.15%. The fluid is put into motion by rotating the top lid using a stepping motor with a precision of 1/2400 RPS. For the present setup and working fluid a Reynolds number of 3000 corresponds to about 1 rotation per second. Thus, for the range of *Re* considered, the variation in angular velocity during a revolution is less than 0.05%.

As the viscosity of the working fluid is very sensitive to temperature changes the viscosity/temperature relation was carefully controlled during the experiments. The fluid temperature was measured within 0.05°C, leading to an uncertainly of 0.2% for the viscosity. The total error of *Re* did not exceed ±10 in a range of Reynolds numbers from 2000 to 5000.

2.2 *Experimental setup*

To measure the spatial-temporal behaviour of the early transition process the high spatial resolution of PIV is combined with the temporal accuracy of LDA.

LDA and PIV are well-known optical experimental techniques for measuring flow velocities. Both methods are non-intrusive and hence do not disturb the investigated flow. The seeding particles do not impose any significant influence on the velocity field. The use of PIV allows accurate simultaneous measurements of a complete velocity field in a 2-dimensional plane and LDA makes it possible to determine onset and frequency content of unsteady flows. Thus, combining the two techniques allows one to determine the frequency content of the various modes appearing in the unsteady flow domain as a function of the control parameters (*h* and *Re*).

The experimental setup is sketched in Fig. 3. In the following the various components of the setup shown in the figure will be referred to as numbers in parentheses. The image of the azimuthal projection of the rotating flow (1), generated by the rotating lid (2), is reflected on a mirror (3) placed at an angle of 45° below of the cavity (see Fig. 3).

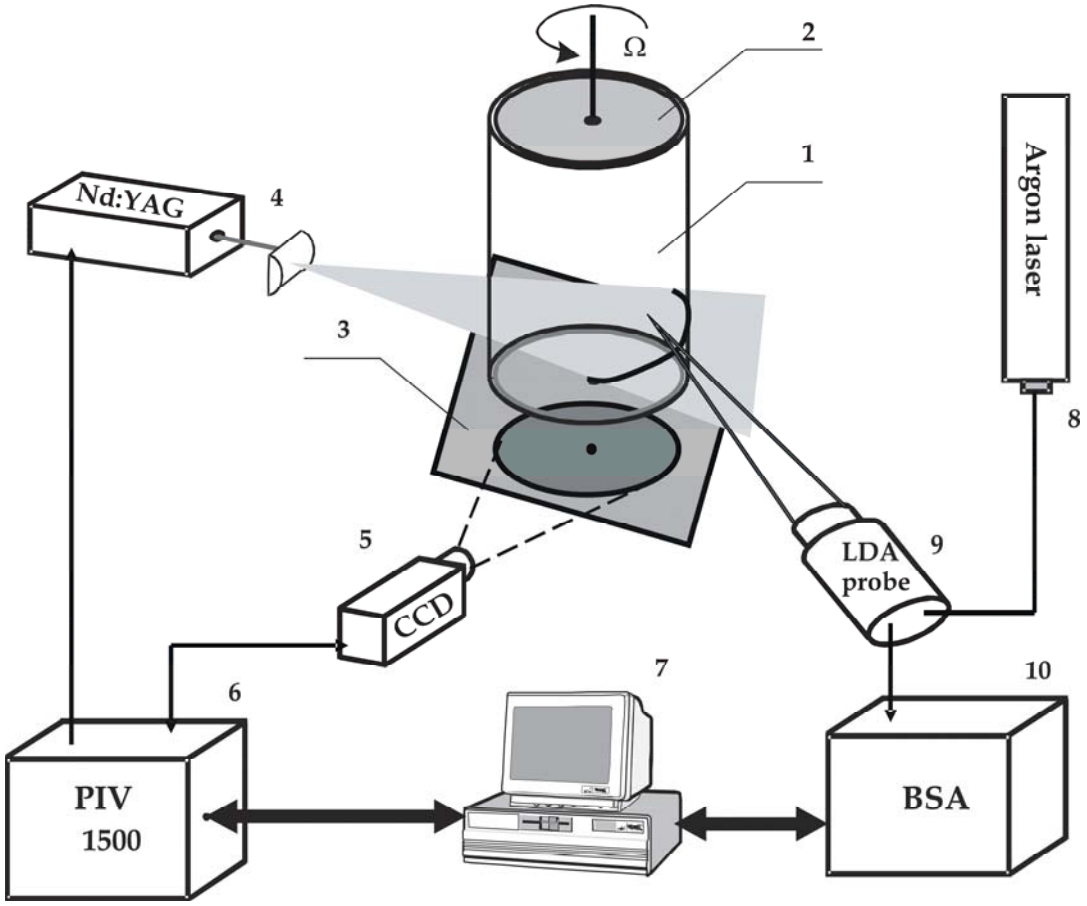

Figure 3. Schematic diagram showing the experimental set-up and instrumentation.

In the PIV measuring system the laser sheet is generated using a pulsed Nd:YAG laser (4) with wavelength λ = 532 nm and pulse energy 50 mJ pulsating at 15 Hz. A plane perpendicular to the axis was illuminated by a laser sheet of thickness ≈3 mm, formed by a combination of spherical and cylindrical lenses. In the experiment a laser sheet at a height of H/4 illuminated a horizontal plane. Images of tracer particles are acquired with a double-buffer high resolution Dantec HiSense camera (5) (1280x1024 pixels, 6.7 μm pixel pitch). A lens with focal length 60 mm fitted with an optical narrow-band filter (532 nm) was used with the camera. A Dantec 1500 FlowMapProcessor (6) carried out synchronization of the lighting system and the camera. A PC (7) equipped with Dantec FlowManager ver. 4.20 was used for acquisition and processing. The interrogation area covered 32x32 pixels with 25% overlapping, providing a spatial resolution of the velocity field of 2.5 mm.

A Dantec 2D Fiber flow LDA (9), based on a 2W Argon laser (8) and a BSA57N2 commercial signal processor (10), was utilized for measuring local velocity histories. In the LDA a two-frequency differential optical configuration with a frequency shift of 40 MHz is applied. The diameter of the optical gauge (9) is 112 mm and the focal length is 600 mm with a beam diameter of 1.35 mm. The wavelengths of laser radiation are 514.5 nm (green light) and 488 nm (blue light). The size of the probing optical field is $0.12\times0.12\times1.52$ mm^3. The signal from light-scattering particles is calculated by the Burst Specter Analyzer (BSA) signal processor (10), collected and processed in the PC (7).

2.3 *Data processing*

Time histories of axial and azimuthal velocity were recorded at various points in the flow field using the LDA. In the present analysis data were collected at (r, z) = (R/4, H/4), (R/2, H/4), (3R/4, H/4) and (R/4, H/2), where r is measured from the center axis and z from the bottom of the cylinder (see Fig. 2). The recorded time histories were analyzed for their frequency content using spectral analysis and compared to the numerical results of Gelfgat et al. (2001). The signals recorded at z = H/4 were further employed to detect the characteristic frequencies of the azimuthal modes. These were subsequently extracted from the processed PIV images. As shown by Gelfgat et al. (2001), the three-dimensional flow instability is most pronounced in the lower part of the cylinder where the rotation is weak and the meridional flow is directed from the sidewall towards the axis. Further, the amplitude of the perturbation of the azimuthal waves is strongest near the sidewall. Each time history was recorded in a period of 60 sec, which was sufficient for determining the frequencies of the modes. To limit the investigation, only wave numbers in the range $k \in [0, 5]$ were analyzed.

The analysis of the PIV images proceeds as follows. First, for each combination of aspect ratio and Reynolds number, (*h, Re*), the mean flow field is determined by averaging 100 randomly recorded PIV images. Next, based on the characteristic frequencies appearing in the LDA samples, time intervals proportional to the time periods of the sought frequencies are defined. In the next step, velocity fields are measured in a time interval consisting of four (for $k \in [0, 3]$) or three (for $k = 4, 5$) oscillation periods. By selecting samples at equidistant time instants, phase averaged velocity fields were obtained by averaging 12-16 PIV samples during a full time interval. As in the stationary case, such a short-period averaging of instantaneous velocity fields reduces potential measurement errors, and almost completely excludes phase errors caused by unsteady changes in the flow structures. In the final step the mean field is subtracted from the phase-averaged PIV samples and, as a result, the modes become visible. Thus, combining LDA and PIV, using the above-described procedure, allows detecting frequencies and associated modes of the underlying flow structures.

3. Results and Discussion

In the following we present some main results of the experiments.

3.1 *Onset of azimuthal waves*

For Reynolds numbers below a certain threshold value the base flow in the lid-driven cylindrical cavity is steady and axisymmetric, that is, it is invariant under rotation by any angle about the cylinder axis. Depending on the aspect ratio and the Reynolds number, the flow gradually becomes unsteady and non-axisymmetric. At a Reynolds number of about 4500, the power spectra become broad-banded after which it becomes difficult to extract modes and frequencies and to distinguish small-scale fluctuations from noise.

The LDA measurements were systematically carried out in the range $h \in [1.0, 3.5]$, starting at $h = 1.0$ with an increasing step size $\Delta h = 0.1$, and in the range $Re \in [2000, 5000]$, starting at $Re = 2000$ and with an increasing step size $\Delta Re = 100$. Next, to detect hystereses phenomena the measurements were repeated by decreasing the Reynolds number. The experimentally observed flow states reveal the occurrence of neutral and critical Reynolds numbers, and associated frequencies, as function of aspect ratio $h \in [1.0, 3.5]$ and wave number $k \in [0,5]$. The frequency is put into dimensionless form, defined as $\omega_k = 2\pi f_k / \Omega$, where Ω is the frequency of the lid and f_k is the frequency of mode k. Using LDA, the sign of ω_k, defined positive when the azimuthal wave is propagating in the same direction as the rotation of the lid, is indefinite and, as a consequence, only the absolute value of ω_k will be shown in the following.

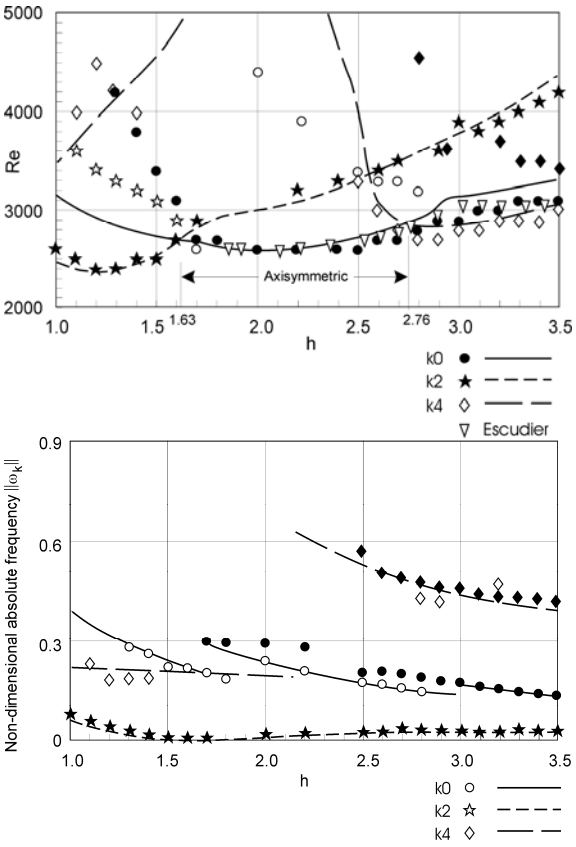

Figur 4. Transition scenario for even modes. Upper: Neutral and critical Reynolds numbers as function of aspect ratio, h, and Reynolds number, Re. Lower: Non-dimensional absolute frequencies.

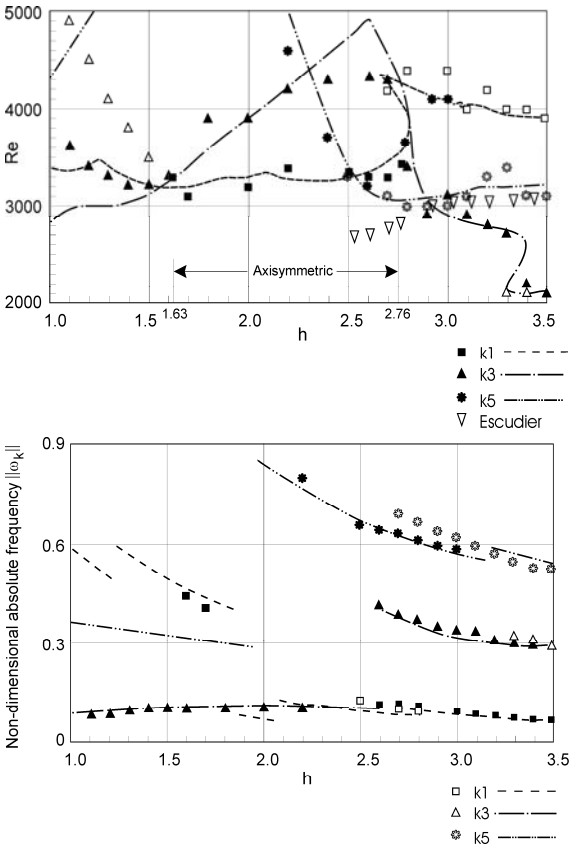

Figur 5. Transition scenario for odd modes. Upper: Neutral and critical Reynolds numbers as function of aspect ratio, h, and Reynolds number, Re. Lower: Non-dimensional absolute frequencies.

The observed neutral and critical Reynolds numbers, and associated frequencies, are plotted in Figs. 4 and 5 and compared to the experimental results for axisymmetric instability of Escudier [3] and the numerical results by Gelfgat et al. [8]. Since we are dealing with a rather large amount of data, the plots are divided into even and odd modes in order to make them easier to grasp. Thus, Fig. 4 depicts distributions of neutral/critical Reynolds numbers and frequencies for even modes and Fig. 5 show the same for odd modes. Further, the region in which Gelfgat et al. [8] observed the dominant perturbation mode to be axisymmetric is inferred with an arrow. Generally, there is a very good agreement between the experiments and simulations shown in Figs. 4 and 5. For example, the agreement between computations and experiments for the low frequency behaviour of the azimuthal mode $k = 2$ is excellent for all investigated aspect ratios (see Fig. 4). It is also remarkable that our experiments in good agreement with the computations predict that the axisymmetric instability is the dominant one in the range $1.6 < h < 2.7$, and that the azimuthal mode $k = 2$ is the dominant one in the range $1.0 < h < 1.6$. Recently, Lopez [9] has carried out a detailed numerical study on the bifurcations appearing at $h = 1.72$. In agreement with our measurements he finds two axisymmetric modes of frequency 0.20 and 0.29 appearing in the range $Re \in [2600, 2700]$ and a $k = 2$ mode of very low frequency appearing at $Re \approx 2900$. In the range $2.7 < h < 3.1$ our measurements show that $k = 4$ is the most unstable mode and that $k = 3$ is the most unstable mode for $3.1 < h < 3.5$. These findings do also agree well with the computations of Gelfgat et al. [8].

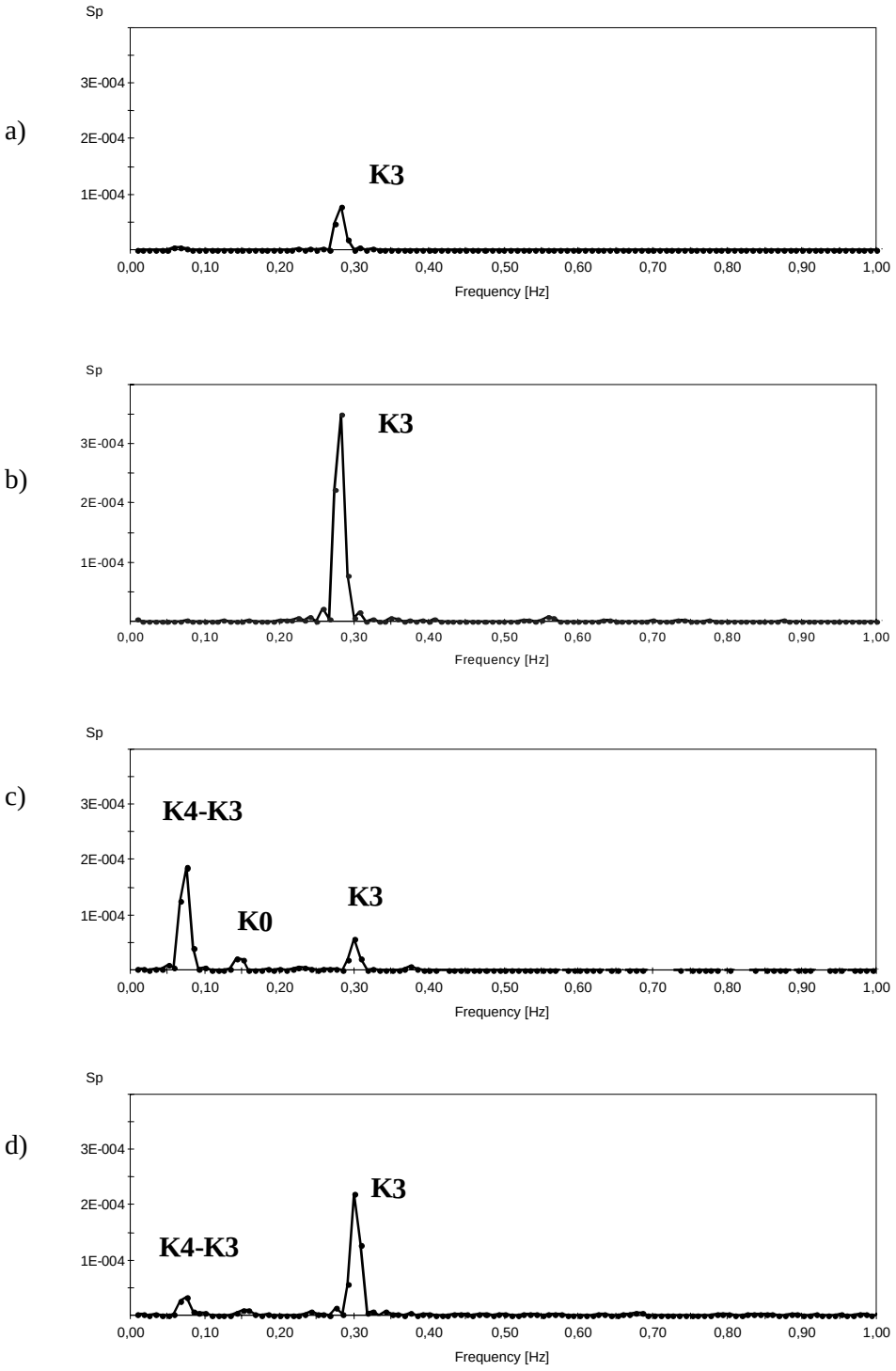

Figure 6. Spectral plots of LDA recordings of azimutal velocities in a lid-driven cylindrical cavity at aspect ratio 3.5. a) (*r*, *z*) = (R/4, H/4) and *Re* = 3000; b) (*r*, *z*) = (3R/4, H/4) and *Re* = 3000; c) (*r*, *z*)=(R/4, H/4) and *Re* = 3100; d) (*r*, *z*)=(3R/4, H/4) and *Re* = 3100.

In the simulations of Gelfgat et al. [8] only the lowest neutral Reynolds numbers were determined for each of the analysed azimuthal modes. Thus, the computations did not reveal further bifurcations in the modes as the Reynolds number was increased. The experimental technique, however, allows us to follow the modes and their associated frequency as the Reynolds number is increased. Therefore, in some cases, especially at high Reynolds numbers and for modes k = 0, 4 and 5, the measurements revealed frequencies that were not captured by the computations.

In Figs. 6a-6d we show spectral plots of measured time histories of the azimutal velocity at (r, z) = (R/4, H/4) and (r, z) = (3R/4, H/4) for Re = 3000 and Re = 3100. Comparing Fig. 6a and Fig. 6b it is seen that the energy of the pulsations of mode k = 3 in the monitor point closest to the vortex bubble is about three times smaller than one appearing in the other monitor point. When the Reynolds number is increased from 3000 to 3100 additional modes k = 0 and k = 4 appear, as seen in Figs. 6c and 6d. Comparing the energy content in the spectra, it is observed that the even modes (k = 0 and k = 4) dominate the inner part of flow domain whereas the outer part is dominated by the odd k = 3 mode.

3.2 *Reconstruction of azimuthal flow fields*

The time histories of the LDA measurements make it is possible to derive the time ranges for averaging instantaneous velocity fields for the PIV method. The resulting perturbed velocity fields were derived by averaging over a series of realizations at divisible time-periods and then subtracting the mean flow field. To illustrate the details of the traveling waves, in the following we show some characteristic azimuthal modes of the perturbed velocity field in a horizontal cross-section z = H/4, measured from the bottom of the cylinder.

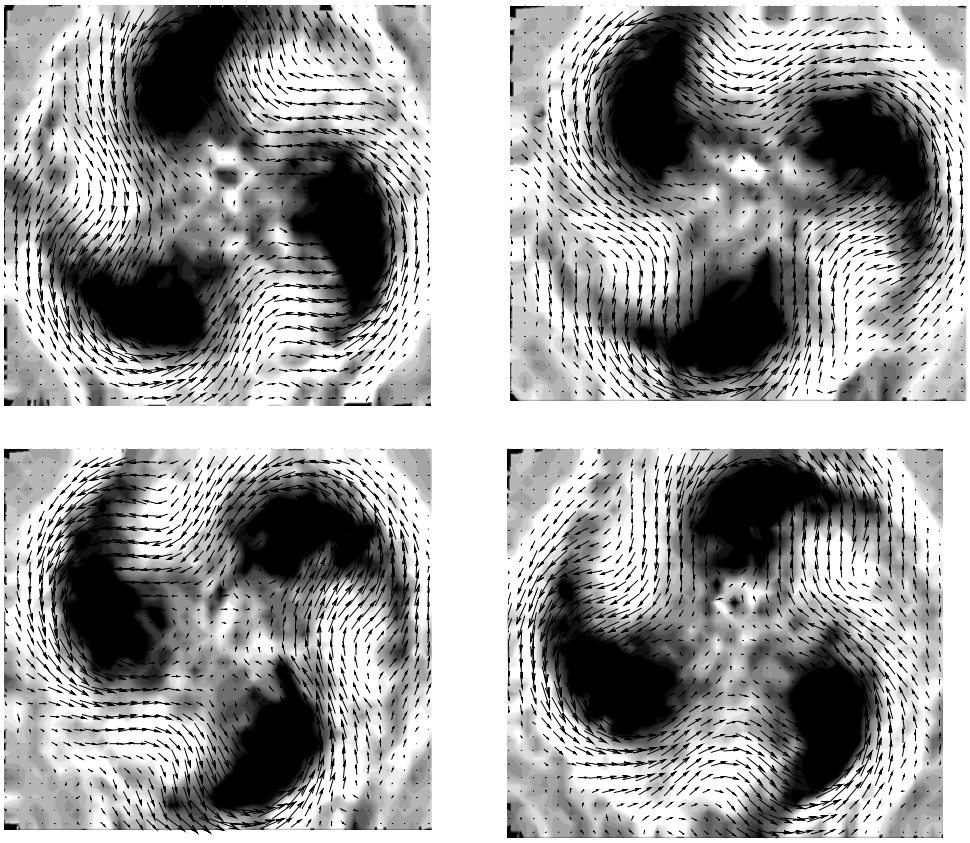

Figure 7. Vorticity and velocity fields at different time phases (T/4) for azimuthal wave k = 3; Reynolds number, Re = 2500, and aspect ratio, h = 3.5. Upper left: Phase t = 0; Upper right: Phase t = T/4; Lower left: Phase t = T/2; Lower right: t = 3T/4.

Fig. 7 shows the vorticity and velocity field of the azimuthal wave for wave number k = 3 at different time phases for h = 3.5 and Re = 2500. In this case the velocity fields were measured in a time period corresponding to four oscillation periods, $4T_{k=3}$, with steps corresponding to a quarter of a period, $T_{k=3}/4$. Thus, for each of the depicted phases, the velocity field is obtained using a statistical average of 12 PIV-samples ($4 \cdot k$), using the procedure described in section 2.3. For the considered regime only the mode k = 3 is active. This allows us to extract a pure k = 3 mode from mean velocity field and depict the movement of the different phases of the wave.

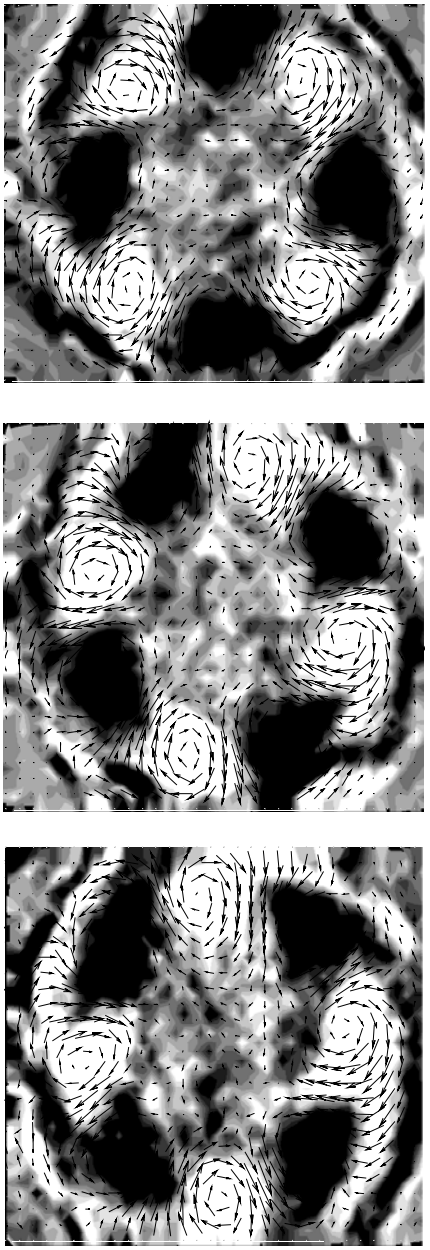

Figure 8. Vorticity and velocity fields at different time phases (T/3) for k=4.

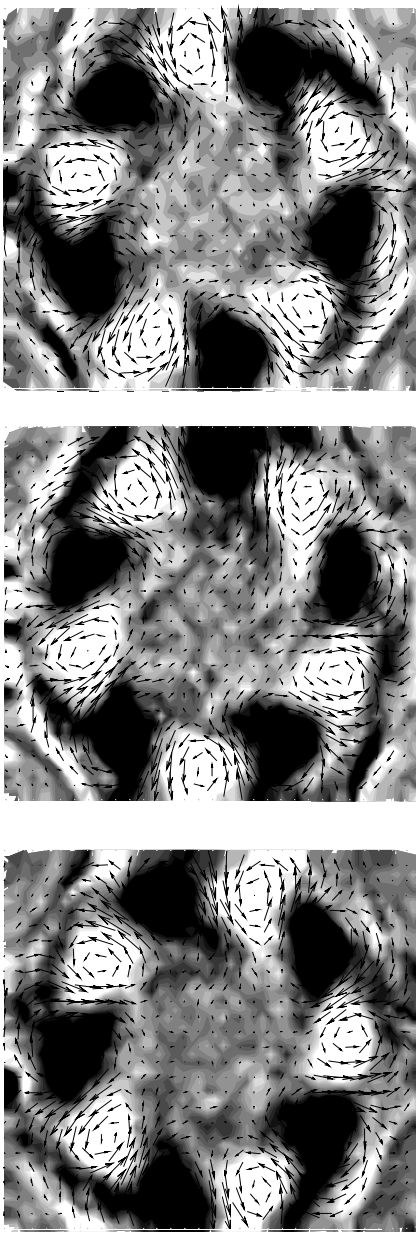

Figure 9. Vorticity and velocity fields at different time phases (T/3) for k=5.

To illustrate the details of the flow conditions for azimuthal waves $k = 4$ and 5, we show the processed PIV images for two representative cases (see Figs. 8 and 9). These cases are in particular a challenge for the averaging technique since all modes are present. Fig. 8 shows vorticity and velocity fields determined from the PIV images of the $k = 4$ mode at $Re = 4400$ and aspect ratio $h = 3.4$. Although all considered modes are present, the averaging technique described above makes it possible to extract the perturbed flow of the azimuthal wave $k = 4$. Fig. 9 shows the resulting vorticity and velocity fields for mode $k = 5$ at $Re = 4300$ and aspect ratio $h = 3.1$.

The experimental investigation confirms the results of Gelfgat et al. [8] that the onset of instability is not connected to vortex breakdown for $3 < h < 3.5$, as the three-dimensional instability in this range sets in before vortex breakdown. Further, the fact that the $k = 4$ mode in the range $2.7 < h < 3.1$ and the $k = 5$ mode in the range $3.1 < h < 3.5$ were not observed by Escudier [3] to be the most dominant modes can be explained from our measurements. Since Escudier only analysed visualizations near the center axis, where recirculation bubbles are likely to appear, he may have overlooked the perturbing non-axisymmetric instabilities that are most dominant near the walls of the cylinder.

4. Conclusions

The onset of unsteady and non-axisymmetric flow behaviour was measured in a closed lid-driven cylindrical cavity for aspect ratios $h \in [1.0, 3.5]$. For the first time, the transition scenario has been experimentally determined using Particle Image Velocimetry (PIV) and Laser Doppler Anemometry (LDA). Combining the high spatial resolution of PIV with the temporal accuracy of LDA allows to extract modes of the dominant azimuthal waves and to map in details the route of transition from steady and axisymmetric flow to unsteady and three-dimensional flow.

The neutral and critical Reynolds numbers, and associated frequencies of the perturbed velocity field, were determined and azimuthal periodicities, patterns and characteristic frequencies of the velocity were extracted and compared to the numerical analysis of Gelfgat et al. [8]. From the experiments it is found that the axisymmetric instability is the dominant one in the range $1.6 < h < 2.7$, and that the azimuthal mode $k = 2$ is dominant in the range $1.0 < h < 1.6$. In the range $2.7 < h < 3.1$ the measurements show that $k = 4$ is the most unstable mode and that $k = 3$ is the most unstable mode for $3.1 < h < 3.5$. These findings are in very good agreement with the computations. Perfect agreement between calculated and measured findings demonstrates the efficiency of using the new diagnostics technique to analyse pulsating vortex flow.

References

[1] Vogel HU 1968 Experimentelle Ergebnisse über die Laminare Strömung in einem zylindrischen Gehäuse mit darin Rotierender Scheibe," *Max-Planck-Institut für Strömungsforschung*, Göttingen, Bericht 6.

[2] Ronnenberg B 1977 Ein selbstjustierendes 3-Komponenten-Laserdoppleranemometer nach dem Vergeichsstrahlvefahren, angewandt auf Untersuchungen in einer stationären zylinder-symmetrischen Drehströmung mit einen Rückströmgebiet," *Max-Planck-Institut für Strömungsforschung*, Göttingen, Bericht 19.

[3] Escudier MP 1984 Observations of the flow produced in a cylindrical container by a rotating endwall. *Exps Fluids* **2** 189-196.

[4] Westergaard CH, Buchhave P, Sørensen JN 1993 PIV measurements of turbulent and chaotic structures in a rotating flow using an optical correlator. In *Laser Techniques and Applications in Fluid Mechanics* (ed. Adrian, RJ), Springer, 243-256.

[5] Spohn A, Mory M, Hopfinger EJ 1998 Experiments on vortex breakdown in a confined flow generated by a rotating disk. *J Fluid Mech* **370** 73-99.

[6] Stevens JL, Lopez JM, Cantwell BJ 1999 Oscillatory flow states in an enclosed cylinder with a rotating endwall. *J Fluid Mech* **389** 101-118.
[7] Sotiropoulos F, Webster DR, Lackey TC 2002 Experiments on Lagrangian transport in steady vortex-breakdown bubbles in a confined swirling flow. *J Fluid Mech* **466** 215-248.
[8] Gelfgat AY, Bar-Yoseph PZ, Solan A 2001 Three-dimensional instability of axisymmetric flow in rotating lid-cylinder enclosure. *J Fluid Mech* **438** 363-377.
[9] Lopez, JM 2006 Rotating and modulated rotating waves in transitions of an enclosed swirling flow. *J Fluid Mech* **553** 323-546.